Non-Hermitian Bulk-Boundary Correspondence and Auxiliary Generalized Brillouin Zone Theory

Zhesen Yang,[1,2,*] Kai Zhang,[1,*] Chen Fang,[1,2,4,†] and Jiangping Hu[1,2,3,‡]

[1]Beijing National Laboratory for Condensed Matter Physics, and Institute of Physics, Chinese Academy of Sciences, Beijing 100190, China

[2]Kavli Institute for Theoretical Sciences, University of Chinese Academy of Sciences, Beijing 100049, China

[3]South Bay Interdisciplinary Science Center, Dongguan, Guangdong 523808, China

[4]Songshan Lake Materials Laboratory, Dongguan, Guangdong 523808, China

(Received 2 February 2020; accepted 29 October 2020; published 24 November 2020)

We provide a systematic and self-consistent method to calculate the generalized Brillouin zone (GBZ) analytically in one-dimensional non-Hermitian systems, which helps us to understand the non-Hermitian bulk-boundary correspondence. In general, a n-band non-Hermitian Hamiltonian is constituted by n distinct sub-GBZs, each of which is a piecewise analytic closed loop. Based on the concept of resultant, we can show that all the analytic properties of the GBZ can be characterized by an algebraic equation, the solution of which in the complex plane is dubbed as auxiliary GBZ (aGBZ). We also provide a systematic method to obtain the GBZ from aGBZ. Two physical applications are also discussed. Our method provides an analytic approach to the spectral problem of open boundary non-Hermitian systems in the thermodynamic limit.

DOI: 10.1103/PhysRevLett.125.226402

Introduction.—Bulk-boundary correspondence (BBC) has played a fundamental role in the development of topological band theory [1–3]. For example, the chiral edge state can be faithfully predicted by the Chern number. A hidden assumption of the celebrated BBC is that the bulk properties of the open boundary condition (OBC) Hamiltonian can be well approximated by the Bloch Hamiltonian with periodic boundary condition (PBC) [4]. However, this hidden assumption is challenged in some non-Hermitian systems recently [5–49]. To be more precise, when the OBC Hamiltonian has non-Hermitian skin effect [5–26], the spectrum between OBC and PBC can be totally distinct [5–13]. It has been revealed that much important information of the OBC Hamiltonian can be encoded from the generalized Brillouin zone (GBZ) [5,6,10,11], which is a generalization of Brillouin zone (BZ) under the OBC in both *Hermitian* and *non-Hermitian* systems. Although the OBC breaks the translational symmetry and the generalization of the BZ seems odd, the basic idea of GBZ is to find a suitable generalized Bloch Hamiltonian (GBZ Hamiltonian) such that the boundary scattering can be regarded as a perturbation. Thus the calculation of GBZ becomes important and has drawn extensive attentions recently [5–20,28–34,50–53]. Unfortunately, up to now, there is no universal analytical method to calculate the GBZ, and the numerical method is not only time consuming but also unreliable due to the existence numerical errors that are extremely sensitive to the lattice size and calculation precision [54,57–59]. In this Letter, we solve this challenging problem analytically based on the concept of auxiliary GBZ (aGBZ). We show that the GBZ of a n-band Hamiltonian has n distinct sub-GBZs, corresponding to the n distinct bands. Each sub-GBZ is a piecewise analytic closed loop, and can be described by a common algebraic equation, namely, the aGBZ equation, which can be calculated based on the concept of resultant of polynomials [54,60–62]. We also provide a systematic method to pick up the GBZ from aGBZ. As applications of our method, we discuss the perturbation-failure effect and the BBC in the case where each band has its respective, distinct sub-GBZ.

BBC and GBZ.—We start from the following one-dimensional (1D) Bloch Hamiltonian:

$$\mathcal{H}(k) = \mathcal{H}_0(k) + i\lambda\mathcal{H}_1(k), \qquad \lambda \in \mathbb{R}, \tag{1}$$

where $\mathcal{H}_{0/1}(k) = \mathcal{H}_{0/1}^{\dagger}(k)$. When $\lambda = 0$, $\mathcal{H}(k)$ becomes Hermitian. As a result, the following discussion is also applicable for the Hermitian case. In general, Eq. (1) with OBC has two different types of nontrivial boundary states, the conventional one that has a Hermitian counterpart, and

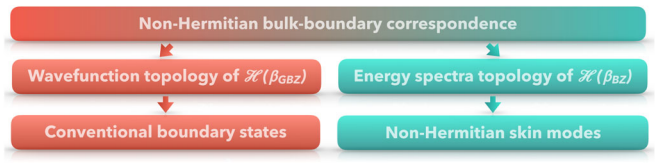

FIG. 1. The non-Hermitian bulk-boundary correspondence has twofold meaning.

the non-Hermitian skin modes without a Hermitian counterpart. Therefore, non-Hermitian Hamiltonians have two different types of BBC as shown in Fig. 1. One relates the conventional boundary state to the wave function topology of the GBZ Hamiltonian $\mathcal{H}(\beta_{\mathrm{GBZ}})$ [5]. Another relates the non-Hermitian skin modes to the (energy) spectra topology of the Bloch Hamiltonian $\mathcal{H}(\beta_{\mathrm{BZ}})$ [11,12]. When the spectra topology is trivial, skin modes do not exist, and GBZ coincides with BZ. As a result, the conventional boundary state can be faithfully predicted by the wave function topology of the Bloch Hamiltonian. Actually, the Hermitian Hamiltonian belongs to this case. However, in general, GBZ and BZ are not identical. In this case, if we want to study the boundary states protected by the wave function topology, the information of GBZ is necessary.

GBZ and aGBZ.—In order to characterize the non-Hermitian skin modes, we first extend the crystal momentum from real numbers to the entire complex plane. Since $\mathcal{H}(k) = \mathcal{H}(k + 2\pi n)$, a natural extension of Eq. (1) is

$$\{\mathcal{H}(k), k \in \mathbb{R}\} \to \{\mathcal{H}(\beta = e^{ik}), k \in \mathbb{C}\}. \tag{2}$$

The eigenvalues of $\mathcal{H}(\beta)$ are determined by the following characteristic equation:

$$f(\beta, E) = \det[E - \mathcal{H}(\beta)] = \frac{P(\beta, E)}{\beta^p} = 0, \tag{3}$$

where p is the order of the pole of $f(\beta, E)$. For example, in the Hatano-Nelson model $\mathcal{H}(\beta) = \mu + t_1\beta + t_{-1}/\beta$ [63], it is obvious that $p = 1$ and $P(\beta, E) = -t_1\beta^2 + (E-\mu)\beta - t_{-1}$. Geometrically, the characteristic equation, Eq. (3), defines a 2D (Riemann) surface in the 4D space $(\beta, E) \in \mathbb{C}^2$. According to $f(\beta, E) = \prod_{\mu=1}^{n}[E - E_\mu(\beta)] = 0$, each energy band (or root) $E = E_\mu(\beta)$ corresponds to a branch of the multivalued function. When the boundary condition is fixed to PBC or OBC, the corresponding Bloch band $(\{E_\mu(\beta_{\mathrm{BZ},\mu}), \mu = 1, \ldots, n\})$ or GBZ band $(\{E_\mu(\beta_{\mathrm{GBZ},\mu}), \mu = 1, \ldots, n\})$ become a set of closed loops on the Riemann surface. As shown in Figs. 2(a) and 3(a), the GBZ is the projection of the GBZ band on the complex β plane.

The aGBZ is defined by the projection of the following two equations on the complex β plane,

$$f(\beta, E) = f(\beta e^{i\theta}, E) = 0, \qquad \theta \in \mathbb{R}. \tag{4}$$

The mathematical meaning of aGBZ is that for a given point β_0 on it with $f(\beta_0, E_0) = 0$, there must exist a conjugate point $\tilde{\beta}_0 = \beta_0 e^{i\theta_0}$ on it satisfying $f(\tilde{\beta}_0, E_0) = 0$ [64]. Therefore, one can define the *root ordering* of $\beta_0 \in \beta_{\mathrm{aGBZ}}$ via the following procedure: (i) solve $f(\beta, E_0) = 0$; (ii) order the roots by the absolute value; (iii) identify the ordering of two roots that have the same absolute value as $|\beta_0|$. For example, if $|\beta_0| = |\beta_m(E_0)| = |\beta_{m+1}(E_0)|$, then,

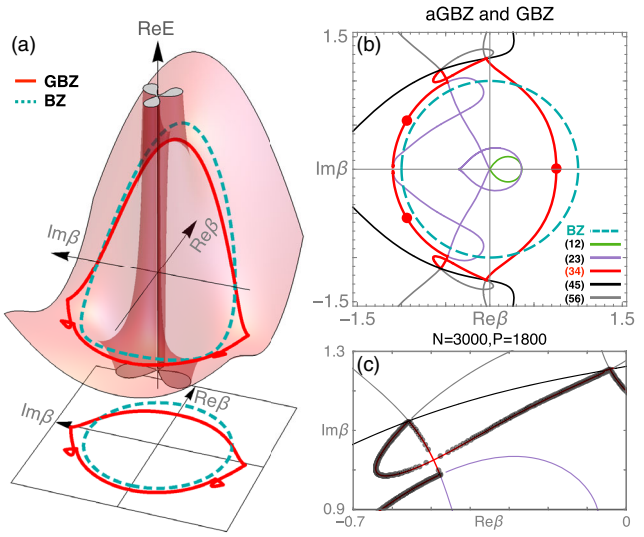

FIG. 2. Non-Hermitian bands, aGBZ, and GBZ of the single band model discussed in the main text. (a) The Bloch band and GBZ band can be regarded as different loops on the 2D surface $f(\beta, E) = 0$. (b) The BZ, aGBZ, and GBZ, where different colors represent different root ordering of the analytic arcs, and the red points represent the self-conjugate points satisfying $\beta_p = \beta_{p+1}$. The GBZ is constituted by the $(p, p+1)$ arcs (red one). (c) The numerical results with $N = 3000$ (lattice size) and $P = 1800$ (digit precision).

$(m, m+1)$ is the root ordering of β_0. This root ordering will be used to pick GBZ from the aGBZ. Since there exist five variables $(\mathrm{Re}\beta, \mathrm{Im}\beta, \mathrm{Re}E, \mathrm{Im}E, \theta)$ and four constraint equations $\mathrm{Re}f = \mathrm{Im}f = \mathrm{Re}f^\theta = \mathrm{Im}f^\theta = 0$, where $f^\theta := f(\beta e^{i\theta}, E)$, the solution of Eq. (4) is a 1D curve in the 5D space. When the additional degrees, θ and E, are eliminated, it can be shown that the constraint equation of the aGBZ is an algebraic equation of $\mathrm{Re}\beta$ and $\mathrm{Im}\beta$,

$$F_{\mathrm{aGBZ}}(\mathrm{Re}\beta, \mathrm{Im}\beta) = \sum_{i,j} c_{ij} (\mathrm{Re}\beta)^i (\mathrm{Im}\beta)^j = 0. \tag{5}$$

In the Supplemental Material [54], we show how to prove Eq. (5) and calculate the coefficients c_{ij} by using the concept of resultant [54,60–62]. The solid lines in Fig. 2(b) with different colors show an example of aGBZ of the following model $\mathcal{H}(\beta) = -1/6 - 1/(2\beta^3) + 8/(5\beta^2) + 10/(3\beta) + 4\beta + 2\beta^2 + \beta^3$. Obviously, the aGBZ is constituted by a set of analytic arcs joined by the self-intersection points.

Now we show how to obtain the GBZ from aGBZ. Notice that any analytic arc on the aGBZ can be labeled by a common root ordering, as shown in Fig. 2(b) with different colors [65]. For the single-band models, the GBZ is constituted by all the arcs labeled by $(p, p+1)$ [11,12], e.g., (3,4) in our example. As shown in Fig. 2(c) and the Supplemental Material [54], our analytical result is consistent with the numerical results with $N = 3000$

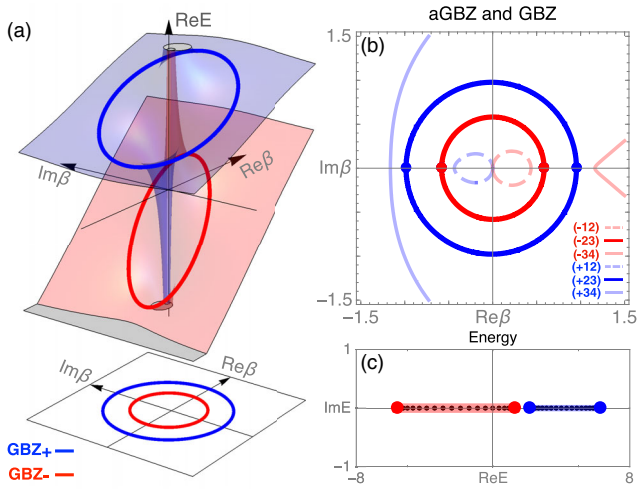

FIG. 3. Non-Hermitian bands, aGBZ, and GBZ of two band model shown in Eq. (6). Different colors in (a) represent different roots in Eq. (7). (b) The aGBZ and GBZ. Each analytic arc on the aGBZ cannot only be labeled by the ordering, but also by the band index. The GBZ is constituted by the $(\pm, 2, 3)$ arcs. (c) The numerical eigenvalues (black points) and GBZ spectra (red and blue lines). The red and blue points in (b) and (c) represent the self-conjugate points ($\beta_p = \beta_{p+1}$) of E_-/E_+ bands, respectively.

(lattice size) and $P = 1800$ (digit precision). However, according to the numerical result, we do not know whether there exist self-intersection points on the GBZ [66]. We note that under the current N and P, the calculation time is 11 days. If we continue to improve the lattice size and numerical accuracy, the calculation time will become unacceptable. We further note that if the calculation precision is not so high ($P = 1800$), the numerical result for $N = 3000$ may become incorrect [54]. This is the central difficulty of the numerical calculation: the numerical diagonalization error of non-Hermitian Hamiltonians is highly sensitive to the matrix size and sometimes may lead to incorrect simulations [54,57–59]. Our analytical method overcomes this difficulty and can be further used to verify the accuracy of numerical calculations. On the GBZ, there exists a set of self-conjugate points satisfying $\tilde{\beta}_p = \beta_{p+1}$, as shown in Fig. 2(b) with red points. A statement about the self-conjugate points is that any analytic arc containing them must form the GBZ. In summary, the aGBZ is a minimal analytic element containing all the information of GBZ and the GBZ is in general a subset of aGBZ.

Generalizing the discussion to the multiband system, we will show that the sub-GBZs for each band can be distinct. Consider the following two-band example,

$$\mathcal{H}(\beta) = \begin{pmatrix} t_0 + t_{-1}/\beta + t_1\beta & c \\ c & w_0 + w_{-1}/\beta + w_1\beta \end{pmatrix}, \quad (6)$$

with $t_0 = 4, t_1 = t_{-1} = 1, w_0 = -2, w_1 = 3, w_{-1} = 1, c = -1$. The eigenvalues of the Hamiltonian are

$$E_\pm(\beta) = h_0(\beta) \pm \sqrt{c^2 + h_z^2(\beta)}, \quad (7)$$

where $h_{0/z}(\beta) = [h_1(\beta) \pm h_2(\beta)]/2$, $h_1(\beta) = t_0 + t_{-1}/\beta + t_1\beta$, $h_2(\beta) = w_0 + w_{-1}/\beta + w_1\beta$. As shown in Fig. 3(a), the red and blue surfaces show the real parts of $E_+(\beta)$ and $E_-(\beta)$, respectively. When the OBC is chosen, $E_\pm(\beta_{\mathrm{GBZ},\pm})$ (red and blue solid lines) define two closed loop on the branches $E_\pm(\beta)$, respectively. As shown in Fig. 3(a), their projections on the complex plane are the multiband GBZ, which is constituted by two distinct sub-GBZs, $\beta_{\mathrm{GBZ},+}$ and $\beta_{\mathrm{GBZ},-}$.

If the multiband Hamiltonian is not block diagonal and has no additional symmetry, the GBZ is also constituted by all the arcs labeled by $(p, p+1)$ [5,10,11,49], e.g., (2,3) in our example with $c \neq 0$. However, if the Hamiltonian is block diagonal, e.g., $c = 0$ in Eq. (6), then, the GBZ is the union of the ones belonging to each nonblock diagonal part, namely, $\beta_{\mathrm{GBZ}} = \beta_{\mathrm{GBZ},1} \cup \beta_{\mathrm{GBZ},2}$ for $c = 0$ in Eq. (6) [67]. We now extract the band information from aGBZ. From the aGBZ (dashed and solid lines) shown in Fig. 3(b), for any point β_0 on the analytic arc, Eq. (7) maps β_0 to $E_+(\beta_0)$ and $E_-(\beta_0)$. By solving $f[\beta, E_\pm(\beta_0)] = 0$ and ordering the roots by the absolute values, one can check which one satisfies the aGBZ condition, that is, there exist two roots having the same absolute values as $|\beta_0|$. Therefore, all the analytic arcs can be further labeled by the band index. For example, the blue and red lines in Fig. 3(b) belong to $E_\pm$ band, respectively. In our example, only the arcs with labeling $(\pm, p, p+1)$ constitute the GBZ. Using Eq. (7) to map $\beta_{\mathrm{GBZ}\pm}$, to $E_\pm(\beta_{\mathrm{GBZ},\pm})$, one can obtain the GBZ spectra shown in Fig. 3(c) with blue and red lines, which matches the numerical results (black dots) [68]. The self-conjugate points (red and blue points) in Figs. 3(b) and 3(c) correspond to the end points of the energy spectra. We finally note that each band, $E_\mu(\beta)$, can only map its own sub-GBZ, $\beta_{\mathrm{GBZ},\mu}$. This fact has a geometrical interpretation: each band dispersion is only defined on each branch of Eq. (3).

Application I: Perturbation failure.—We now show some applications of the aGBZ theory. The first one is the perturbation-failure (or critical skin) effect in non-Hermitian band theory [69,70]. As shown in Figs. 4(a) and 4(b), when we choose $t_0 = 1, t_1 = 1, t_{-1} = 2$, $w_0 = -1, w_1 = 3, w_{-1} = 1$ in Eq. (6), the OBC spectrum (dots) of $c = 0$ and $c = 1/100$ exhibits a nonperturbative behavior [71]. With the increasing of lattice size N, the nonperturbative effect becomes stronger. The aGBZ theory not only provides an analytical method to understand this phenomenon, but also can strictly prove the discontinuity of the energy spectrum evolution at $c = 0$ under the thermodynamic limit [72]. As shown in Figs. 4(c) and 4(d), when $c = 0$ and $c = 0^+$ (right-hand limit), the aGBZ of Eq. (6) are the same, namely, $\beta_{\mathrm{aGBZ}}(c = 0) = \beta_{\mathrm{aGBZ}}(c = 0^+)$. However, when c changes from zero to nonzero, the GBZ condition is changed. To be

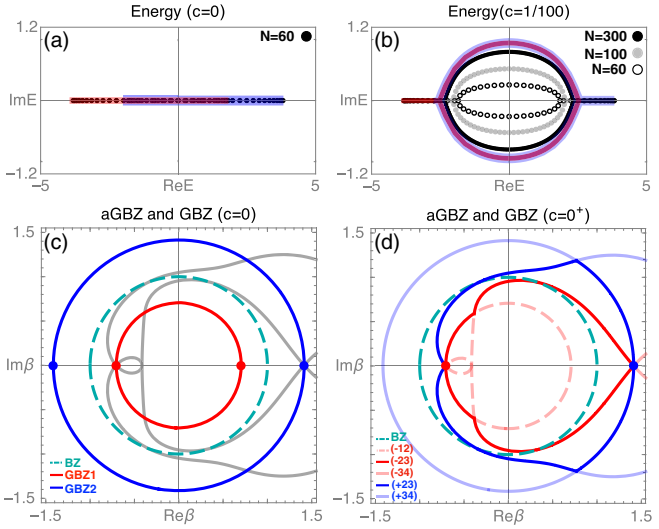

FIG. 4. Perturbation-failure (or critical skin) effect. The nonperturbative behavior of the OBC spectrum between $c = 0$ [dots in (a)] and $c = 1/100$ [dots in (b)] of Eq. (6) can be understood by the discontinuity of GBZ (red and blue opaque solid lines) in (c) and (d), namely, $\beta_{\mathrm{GBZ}}(c = 0) \neq \beta_{\mathrm{GBZ}}(c = 0^+)$. The solid lines in (a) and (b) represent the analytic GBZ spectrum $E_{\mathrm{GBZ}}(c = 0)$ and $E_{\mathrm{GBZ}}(c = 0^+)$, respectively.

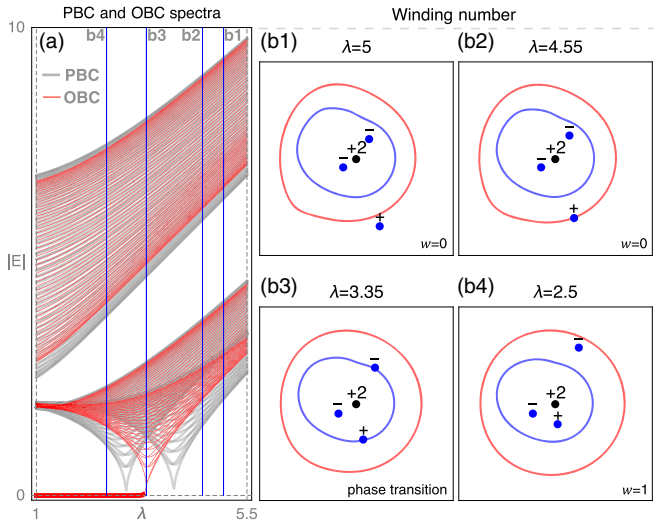

FIG. 5. Wave function winding number and nondegenerate sub-GBZs of Eq. (8). (a) The PBC/OBC spectrum $|E|$ as a function of λ. (b) The evolution of the GBZ, topological charge, and winding number. Red and blue lines represent two distinct sub-GBZs. The total winding number equals one-half of the charge summation of the black dot and the blue dots inside the blue sub-GBZ.

more precise, when $c = 0$, Eq. (6) is diagonal and the characteristic equation $f(\beta, E) = [E - h_1(\beta)][E - h_2(\beta)]$ is *reducible*. The asymptotic solutions are determined by the two separated irreducible polynomials $E - h_1(\beta)$ and $E - h_2(\beta)$, which result two independent sub-GBZs, $\beta_{\mathrm{GBZ},1} = \sqrt{t_{-1}/t_1}e^{ik}$ and $\beta_{\mathrm{GBZ},2} = \sqrt{w_{-1}/w_1}e^{ik}$, as shown in Fig. 4(c). However, when $c \to 0^+$, these two bands will couple together and the GBZ is determined by the irreducible polynomial $f(\beta, E) = [E - h_1(\beta)][E - h_2(\beta)] - c^2$. As a result, only the $(\pm, 2, 3)$ arcs on the aGBZ constitute the GBZ, as shown in Fig. 4(d). Comparing (c) and (d), it is obvious $\beta_{\mathrm{GBZ}}(c=0) \neq \beta_{\mathrm{GBZ}}(c=0^+)$, which implies $E_{\mathrm{GBZ}}(c=0) \neq E_{\mathrm{GBZ}}(c=0^+)$ as shown by the solid lines in Figs. 4(a) and 4(b), respectively.

Application II: wave function winding number.—The second application of the aGBZ theory is the BBC in the case where each band has its respective, distinct sub-GBZ. Consider the following *four-band* model preserving sublattice symmetry [73],

$$\mathcal{H}(\beta) = \begin{pmatrix} 0 & R_+(\beta) \\ R_-(\beta) & 0 \end{pmatrix}, \tag{8}$$

where $R_\pm(\beta) = \lambda + (t_\pm + t_1\beta^{\pm 1})\sigma_\pm + t_2\beta^{\pm 1}\sigma_\mp$ and $t_1 = 2$, $t_2 = 2i, t_\pm = 5 \pm 2$. Since the Hamiltonian has sublattice symmetry, the eigenvalues come in pairs, e.g., $(E, -E)$. As a result, the sub-GBZs of $E_\mu(\beta)$ and $-E_\mu(\beta)$ must be degenerate [74]. Figure 5(a) shows the differences between the OBC-PBC spectrum ($|E|$) as λ evolves. In order to characterize the emergence of topological zero modes in (a), we need to define the (wave function) winding number of the GBZ Hamiltonian $\mathcal{H}(\beta_{\mathrm{GBZ}})$. However, due to the existence of multiple sub-GBZs shown in Fig. 5(b), the definition based on the Q matrix [5,10] cannot be extended directly [75]. We note that once the root of $\det[\mathcal{H}(\beta)] = 0$ passes through the GBZ, it *may* correspond to a topological phase transition. Therefore, it can be regarded as a topological charge. According to $\det[\mathcal{H}(\beta)] = \det[R_+(\beta)]\det[R_-(\beta)] = E_1^2(\beta)E_2^2(\beta) = 0$, the zeros can be labeled by the R index $\pm$, which determine the sign of the charge, and band index $\mu = 1, 2$, which is related to the sub-GBZs. When the zeros belonging to the first band ($E_1(\beta) = 0$) cross the sub-GBZ of second band ($\beta_{\mathrm{GBZ},2}$), as shown in Fig. 5(b2) where the colors represent the band index, there is no gap closing and phase transition. This inspires us to write down the following conjectured formula [54]:

$$w = \frac{1}{2}(w_+ - w_-), \qquad w_\pm = -P_\pm + \sum_{\mu=1}^{m} Z_{\pm,\mu}, \tag{9}$$

where $Z_{\pm,\mu}$ are the number of zeros not only satisfying $\det[R_\pm(\beta)] = E_\mu(\beta) = 0$ but also being inside the sub-GBZ $\beta_{\mathrm{GBZ},\mu}$, and $P_\pm$ are the orders of the pole of $\det[R_\pm(\beta)]$. As shown in Fig. 5(b), we plot the GBZ and the topological charges for different values of λ, where the black dots represent the charge of pole, namely, $P_+ = 0$ and $P_- = 2$; the blue dots with charge $\pm$ represent the zeros belonging to the blue sub-GBZ band and satisfying $\det[R_\pm(\beta)] = 0$. Since there are no zeros belonging to the red sub-GBZ band

under the parameters shown in (b), the total winding number equals one-half of the charge summation of the black dot and the blue dots inside the blue sub-GBZ. This result is consistent with Fig. 5(a).

Discussions and conclusions.—In summary, we have provided an analytical method to calculate the GBZ, which acts as the role of the exact solution of non-Hermitian OBC Hamiltonians in the thermodynamic limit. Compared with the previous numerical methods, our work reduces the problem to the task of calculating the resultant and solving algebraic equations, the process of which is faster and error-free.

This work is supported by the Ministry of Science and Technology of China (No. 2016YFA0302400, No. 2017YFA0303100), the National Science Foundation of China (Grants No. NSFC-11888101, No. 11674370), Chinese Academy of Sciences (No. XXH13506-202 and XDB33000000), and the Strategic Priority Research Program of CAS (Grant No. XDB28000000).

*These authors contributed equally to this work.
†Corresponding author.
cfang@iphy.ac.cn
‡Corresponding author.
jphu@iphy.ac.cn

[1] M. Z. Hasan and C. L. Kane, Rev. Mod. Phys. **82**, 3045 (2010).
[2] X.-L. Qi and S.-C. Zhang, Rev. Mod. Phys. **83**, 1057 (2011).
[3] B. A. Bernevig and T. L. Hughes, *Topological Insulators and Topological Superconductors, student edition* (Princeton University Press, Princeton, NJ, 2013).
[4] A. Alase, E. Cobanera, G. Ortiz, and L. Viola, Phys. Rev. Lett. **117**, 076804 (2016).
[5] S. Yao and Z. Wang, Phys. Rev. Lett. **121**, 086803 (2018).
[6] S. Yao, F. Song, and Z. Wang, Phys. Rev. Lett. **121**, 136802 (2018).
[7] F. Song, S. Yao, and Z. Wang, Phys. Rev. Lett. **123**, 170401 (2019).
[8] F. Song, S. Yao, and Z. Wang, Phys. Rev. Lett. **123**, 246801 (2019).
[9] F. K. Kunst, E. Edvardsson, J. C. Budich, and E. J. Bergholtz, Phys. Rev. Lett. **121**, 026808 (2018).
[10] K. Yokomizo and S. Murakami, Phys. Rev. Lett. **123**, 066404 (2019).
[11] K. Zhang, Z. Yang, and C. Fang, Phys. Rev. Lett. **125**, 126402 (2020).
[12] N. Okuma, K. Kawabata, K. Shiozaki, and M. Sato, Phys. Rev. Lett. **124**, 086801 (2020).
[13] Y. Xiong, J. Phys. Commun. **2**, 035043 (2018).
[14] V. M. Martinez Alvarez, J. E. Barrios Vargas, and L. E. F. Foa Torres, Phys. Rev. B **97**, 121401(R) (2018).
[15] C. H. Lee and R. Thomale, Phys. Rev. B **99**, 201103(R) (2019).
[16] S. Longhi, Opt. Lett. **44**, 5804 (2019).
[17] L. Herviou, J. H. Bardarson, and N. Regnault, Phys. Rev. A **99**, 052118 (2019).
[18] H.-G. Zirnstein, G. Refael, and B. Rosenow, arXiv: 1901.11241.
[19] H. Jiang, L.-J. Lang, C. Yang, S.-L. Zhu, and S. Chen, Phys. Rev. B **100**, 054301 (2019).
[20] S. Longhi, Phys. Rev. Research **1**, 023013 (2019).
[21] K.-I. Imura and Y. Takane, Phys. Rev. B **100**, 165430 (2019).
[22] T. Helbig, T. Hofmann, S. Imhof, M. Abdelghany, T. Kiessling, L. W. Molenkamp, C. H. Lee, A. Szameit, M. Greiter, and R. Thomale, Nat. Phys. **16**, 747 (2020).
[23] L. Xiao, T. Deng, K. Wang, G. Zhu, Z. Wang, W. Yi, and P. Xue, Nat. Phys. **16**, 761 (2020).
[24] T. Hofmann, T. Helbig, F. Schindler, N. Salgo, M. Brzezińska, M. Greiter, T. Kiessling, D. Wolf, A. Vollhardt, A. Kabaši, C. H. Lee, A. Bilušić, R. Thomale, and T. Neupert, Phys. Rev. Research **2**, 023265 (2020).
[25] X. Zhang and J. Gong, Phys. Rev. B **101**, 045415 (2020).
[26] L. Li, C. H. Lee, and J. Gong, Phys. Rev. Lett. **124**, 250402 (2020).
[27] L. E. F. F. Torres, J. Phys. **3**, 014002 (2019).
[28] D. S. Borgnia, A. J. Kruchkov, and R.-J. Slager, Phys. Rev. Lett. **124**, 056802 (2020).
[29] W. Brzezicki and T. Hyart, Phys. Rev. B **100**, 161105 (2019).
[30] T.-S. Deng and W. Yi, Phys. Rev. B **100**, 035102 (2019).
[31] E. Edvardsson, F. K. Kunst, and E. J. Bergholtz, Phys. Rev. B **99**, 081302(R) (2019).
[32] M. Ezawa, Phys. Rev. B **99**, 121411(R) (2019).
[33] F. K. Kunst and V. Dwivedi, Phys. Rev. B **99**, 245116 (2019).
[34] H. Wang, J. Ruan, and H. Zhang, Phys. Rev. B **99**, 075130 (2019).
[35] K. Kawabata, K. Shiozaki, M. Ueda, and M. Sato, Phys. Rev. X **9**, 041015 (2019).
[36] Z. Gong, Y. Ashida, K. Kawabata, K. Takasan, S. Higashikawa, and M. Ueda, Phys. Rev. X **8**, 031079 (2018).
[37] L. Li, C. H. Lee, and J. Gong, Phys. Rev. B **100**, 075403 (2019).
[38] H. Shen, B. Zhen, and L. Fu, Phys. Rev. Lett. **120**, 146402 (2018).
[39] N. Okuma and M. Sato, Phys. Rev. Lett. **123**, 097701 (2019).
[40] L. Jin and Z. Song, Phys. Rev. B **99**, 081103(R) (2019).
[41] K. Takata and M. Notomi, Phys. Rev. Lett. **121**, 213902 (2018).
[42] S. Longhi, Phys. Rev. Lett. **124**, 066602 (2020).
[43] A. Ghatak and T. Das, J. Phys. Condens. Matter **31**, 263001 (2019).
[44] V. M. Martinez Alvarez, J. E. Barrios Vargas, M. Berdakin, and L. E. F. Foa Torres, Eur. Phys. J. Special Topics **227**, 1295 (2018).
[45] J. M. Zeuner, M. C. Rechtsman, Y. Plotnik, Y. Lumer, S. Nolte, M. S. Rudner, M. Segev, and A. Szameit, Phys. Rev. Lett. **115**, 040402 (2015).
[46] M. S. Rudner and L. S. Levitov, Phys. Rev. Lett. **102**, 065703 (2009).
[47] S. Lieu, Phys. Rev. B **97**, 045106 (2018).
[48] D. C. Brody, J. Phys. A **47**, 035305 (2014).
[49] Y. Yi and Z. Yang, Phys. Rev. Lett. **125**, 186802 (2020).
[50] T. E. Lee, Phys. Rev. Lett. **116**, 133903 (2016).

[51] D. Leykam, K. Y. Bliokh, C. Huang, Y. D. Chong, and F. Nori, Phys. Rev. Lett. **118**, 040401 (2017).
[52] V. M. Martinez Alvarez, J. E. Barrios Vargas, M. Berdakin, and L. E. F. Foa Torres, Eur. Phys. J. Special Topics **227**, 1295 (2018).
[53] A. Ghatak and T. Das, J. Phys. Condens. Matter **31**, 263001 (2019).
[54] See Supplemental Material at http://link.aps.org/supplemental/10.1103/PhysRevLett.125.226402 for (i) difficulties in numerical calculation of the generalized Brillouin zone, (ii) calculation of the auxiliary generalized Brillouin zone, (iii) some details of the single-band model in the main text, (iv) wave function winding number in the multiple sub-GBZ cases, (v) the Mathematica code, which includes additional Refs. [55,56].
[55] K. Kawabata, N. Okuma, and M. Sato, Phys. Rev. B **101**, 195147 (2020).
[56] Z. Yang, C.-K. Chiu, C. Fang, and J. Hu, Phys. Rev. Lett. **124**, 186402 (2020).
[57] M. J. Colbrook, B. Roman, and A. C. Hansen, Phys. Rev. Lett. **122**, 250201 (2019).
[58] A. Böttcher and S. M. Grudsky, *Spectral Properties of Banded Toeplitz Matrices*, Vol. 96 (Siam, Philadelphia, 2005).
[59] L. Reichel and L. N. Trefethen, Linear Algebra Appl. **162–164**, 153 (1992).
[60] Wikipedia, 2019, page Version ID: 905762282.
[61] H. Woody, Polyn. Resultants 10 (2016), http://buzzard.ups.edu/courses/2016spring/projects/woody-resultants-ups-434-2016.pdf.
[62] S. Janson, *Resultant and Discriminant of Polynomials* (2010), Vol. 18, http://www2.math.uu.se/~svante/papers/sjN5.pdf.
[63] N. Hatano and D. R. Nelson, Phys. Rev. Lett. **77**, 570 (1996).
[64] In general, β_0 and $\tilde{\beta}_0$ are different points on the aGBZ.
[65] The reason is that for any point on the analytic arcs, the root ordering can only be changed at the self-intersection points.
[66] We note that this kind of self-intersection point is a new type of singularity point, which has no counterpart in Hermitian systems and is unique to non-Hermitian systems. The details have been discussed in the Supplemental Material [54].
[67] It can be shown that $\beta_{\mathrm{GBZ},1} = \sqrt{t_{-1}/t_1}e^{ik}$ and $\beta_{\mathrm{GBZ},2} = \sqrt{w_{-1}/w_1}e^{ik}$ for the parameters we have chosen, i.e., $t_0 = 4, t_1 = t_{-1} = 1, w_0 = -2, w_1 = 3, w_{-1} = 1$.
[68] We note that $\beta_{\mathrm{GBZ},+}$ can only be mapped by $E_+(\beta)$ and the corresponding GBZ spectra for E_+ band becomes $E_+(\beta_{\mathrm{GBZ},+})$. While the GBZ spectra for E_- band becomes $E_-(\beta_{\mathrm{GBZ},-})$.
[69] N. Okuma and M. Sato, Phys. Rev. Lett. **123**, 097701 (2019).
[70] L. Li, C. H. Lee, S. Mu, and J. Gong, arXiv:2003.03039.
[71] This means the spectra change is lager than the perturbation strength.
[72] We note that the GBZ and the corresponding GBZ spectra $E_\mu(\beta_{\mathrm{GBZ},\mu})$ are defined in the thermodynamic limit.
[73] K. Kawabata, K. Shiozaki, M. Ueda, and M. Sato, Phys. Rev. X **9**, 041015 (2019).
[74] This is because the characteristic equation of the non-Bloch Hamiltonian preserving sublattice symmetry satisfies $f(\beta, E) = f(\beta, -E)$ [49].
[75] The reason is that the Q matrix is defined on all occupied bands, it is not clear which sub-GBZs should be chosen as the integration path. In the Supplemental Material [54], we provide a detailed discussion.